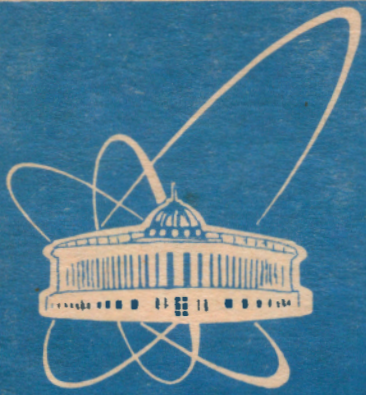

ОБЪЕДИНЕННЫЙ
ИНСТИТУТ
ЯДЕРНЫХ
ИССЛЕДОВАНИЙ

Дубна

95-30

E5-95-30

M.Bondila[1], I.V.Barashenkov[2], M.M.Bogdan[1,3]

TOPOGRAPHY OF ATTRACTORS OF THE PARAMETRICALLY DRIVEN NONLINEAR SCHRÖDINGER EQUATION

Submitted to «Physica D»

[1]Department of Mathematics, University of Cape Town, Private Bag Rondebosch 7700, South Africa.
Internet: bndmar07@uctvax.uct.ac.za
[2]Address after 1.02.1995: Theoretische Natuurkunde, Fakulteit der Wetenschappen, Vrije Universiteit Brussel, 1050 Brussel, Belgium.
E-mail: igor@main1.jinr.dubna.su
[3]On leave of absence from Institute for Low Temperature Physics and Technology, 47 Lenin Avenue, Kharkov 310164, Ukraine.
E-mail: bogdan@ilt.kharkov.ua

1995

A large number of nonlinear resonant phenomena in various physical media is described by the parametrically driven, damped nonlinear Schrödinger equation [1, 2, 3]:

$$i\psi_t + \Delta\psi + 2|\psi|^2\psi = h\psi^* e^{2i\Omega t} - i\gamma\psi. \tag{1}$$

These include the Faraday resonance in fluid dynamics [4], the parametric generation of spin waves in ferro and antiferromagnets [1, 5], instabilities in plasma [6, 7] and the amplitude modulation in Josephson junctions [8]. In all these cases, a strong parametric excitation of the system can produce and sustain solitonic waves [2, 3, 9].

Stability of the parametrically excited solitons heavily depends on the dimensionality of space and geometry of the problem at hand. Solitons in three-dimensional unbounded systems were shown to be unstable and to collapse in a finite time [1, 10]. However, if the system is bounded in one or two directions (consider, for instance, a long narrow rectangular water tank [4]), a stable soliton can be experimentally observed. Provided this soliton is exponentially localised only in one direction, it behaves as an effectively one-dimensional object [2]. There are also a number of genuinely one-dimensional physical systems such as the one-dimensional ferro and antiferromagnets and long Josephson junctions where the existence of the parametrically driven soliton was predicted [11, 3]. All this motivates the study of the *one-dimensional* version of eq. (1) which this Letter is devoted to. Our objective here is to explore the complexity in the internal dynamics of the parametrically driven NLS soliton, and to examine the existence of other (localised and extended) attractors.

By means of a simple scaling we can always arrange that $\Omega = 1$ in eq. (1):

$$i\psi_t + \psi_{xx} + 2\,|\psi|^2\psi = h\psi^* e^{2it} - i\gamma\psi. \tag{2}$$

Here $h > 0$ and $\gamma > 0$ are the driver's strength and dissipation coefficient, respectively. Next the substitution $\psi = e^{it}\phi$ produces an autonomous equation,

$$i\phi_t + \phi_{xx} - \phi + 2\,|\phi|^2\phi = h\phi^* - i\gamma\phi. \tag{3}$$

The simplest solution of eq. (3) is the trivial one, $\phi \equiv 0$, which proves to be stable

for $h < (1+\gamma^2)^{1/2}$ and therefore, acts as an attractor in this region. Consequently we refer to this solution as to the *zero* attractor.

Another explicit solution existing for $h > \gamma$, is the soliton:

$$\phi_s(x,t) = \frac{A_0}{\cosh A_0 x} e^{-i\theta_0},$$
$$A_0 = \sqrt{1 + h\cos 2\theta_0},$$
$$\theta_0 = \frac{1}{2}\arcsin\frac{\gamma}{h}. \qquad (4)$$

Stability of this solution was studied earlier and its stability domain was fully described (see the blank area in Fig. 1) [3, 12]. Above the curve $h = (1+\gamma^2)^{1/2}$ the soliton is unstable with respect to continuous spectrum waves which are excited by the parametric pumping. The soliton has two internal oscillation modes, the resonance of which produces the Hopf bifurcation and instability (line 1 in Fig. 1) [3]. Hence, above the line 1 the soliton is unstable with respect to a localised mode. In ref. [3] it was suggested that this is the first bifurcation in a sequence leading to a temporal chaotic behavior [13].

In this Letter we present numerical studies of nonlinear oscillations and chaotic dynamics of the soliton above the Hopf bifurcation curve (i. e. in the region where the stationary soliton is unstable). We also uncover other attractors in that region and consequently, reconstruct the attractor chart on the (h,γ)-plane.

The evolution of the (unstable) stationary soliton (4) was simulated by the split-step pseudospectral method. The method is a generalisation of the one proposed by Herbst and Weideman [14]. We took 1024 Fourier modes with the time increment $\Delta t = 2\pi \cdot 10^{-3}$. The method imposes periodic boundary conditions $\psi(-L/2) = \psi(L/2)$, $\psi_x(-L/2) = \psi_x(L/2)$ where the interval length was chosen to be $L = 50$.

The main results of our work are summarised in Fig. 1. This is the attractor chart of the parametrically driven NLS on the (h,γ) plane. The region where the stationary soliton is stable was discussed above, while in the unstable region, the following subregions were identified.

First of all, clearly seen is the domain where the period-doubling route to (temporal) chaos takes place. Above the line 1, in the domain marked by open circles, the nontrivial attractor is temporally periodic. Very roughly one may think of it as of a soliton with periodically varying amplitude and phase. (However, unlike the stationary soliton (4), this periodic soliton has undulations on its spatial "tails".) In the vicinity of the curve 1 the frequency of the periodic solution, ω_1, was seen to be in a good agreement with $\mathrm{Im}\,\lambda$ where λ is the complex eigenvalue of the operator arising in the linearisation of eq. (3) around the stationary soliton (4) [3]. In fig. 1, attractors resulting from the subsequent period-doubling (2-periodic, 4-periodic, 8- and higher periodic, and finally, complex cycles and strange attractors) occupy a narrow band of boxes, diamonds and white blobs. The curve 2 is a boundary of the period-doubling sequence and separates the region of strange attractors from the region where only the zero attractor exists. The latter region is marked by empty triangles.

Crossing the bifurcation line 3, the limit cycle is replaced by the spatio-temporal chaos. As opposed to the period-doubling scenario, there are no intermediate attractors here which corresponds to the quasiperiodic route. The line 4 is the interface between the spatio-temporal chaos and the region of the zero attractor. The lines 2, 3 and 4 meet at a "tricritical" point $\gamma_c = 0.25$, $h_c = 0.81$ which separates the period-doubling and quasiperiodic routes.

Details of the period-doubling transition are presented in Figs. 2 and 3. Fig. 2 displays an enlarged portion of the attractor chart exhibiting the period-doubling sequences for the fixed γ and varied h. (Note the appearance of odd periods and their doublings in the neighborhood of the upper boundary of the period-doubling sequence.) In Fig. 3, typical attractors are illustrated by their power spectra. As an example, we have chosen the sequence arising along the line $\gamma = 0.26$. In the vicinity of the curve 1 in Fig. 1 the main harmonic in the power spectrum of the period-1 solution has the frequency $\omega_1 = 1.105$ which practically coincides with $\mathrm{Im}\,\lambda$ (described above.) In this region internal oscillations of the soliton have small amplitudes and a contribution of higher harmonics is negligible. As h is increased,

the main frequency decreases (Figs. 3, a-d) whereas the linearised eigenvalue grows. This implies the growth of anharmonic effects. (Note the growth of amplitudes of multiple harmonics in Figs. 3, b-c.) The period doubling can be seen from the appearance of subharmonics in Fig. 3.

In order to emphasize the existence of the entire Feigenbaum sequence of direct and reverse bifurcations, we plot the phase portrait of a two-band strange attractor arising for $\gamma = 0.26$, $h = 0.4539$ (Fig. 4). The two-band structure is explicitly illustrated by a one-dimensional map $X_{n+2} = f(X_n)$ (Fig. 4b). Here $\{X_n\}$ is the sequence of the maximum values of $\mathrm{Im}\,\psi(0,t)$ on the phase portrait (Fig. 4a).

The band of strange attractors borders the region of the zero attractor. As we approach the border between the two regions, the structure of the strange attractor becomes more complex. This is exemplified by the phase portrait and one-dimensional map of a complex strange attractor for $\gamma = 0.18$ and $h = 0.253$ (Figs. 4, c-d). As h is increased, the strange attractors undergo a crisis (Fig. 4e) and we find ourselves in the zero attractor domain. Thus, the final stage of the soliton's instability following the period-doubling sequence, is its decay to zero. If we increase h for a fixed γ (provided γ is smaller than $\gamma_c = 0.25$ so that we do not cross the upper part of the period-doubling band), the zero attractor becomes unstable and a spatio-temporal chaotic state emerges.

For all $\gamma > \gamma_c$ and $h > h_c$, the transition to chaos is via the quasiperiodic route. In terms of the equation (3) this implies the sequence "stationary soliton → period-1 soliton → spatio-temporal chaos". In terms of eq. (2), the stationary soliton (4) becomes periodic with the frequency of the driver, $\Omega = 1$, while the period-1 soliton becomes quasiperiodic with two frequencies, Ω and ω_1. (Hence the name of the route.) In the vicinity of the curve 4 (the curve of the quasiperiodic transition), an additional low frequency $\tilde{\omega}$ is excited in the power spectrum. Below the curve the low frequency oscillation dies off as a transient. For example, for $\gamma = 0.34$ and $h = 0.994$, the frequency $\tilde{\omega} \approx 0.05$ disappeared from the spectrum after $t \sim 6000$. Above the curve 4, the $\tilde{\omega}$ is also nucleated in the spectrum at the first instance of time — together with combinations of $\tilde{\omega}$ and ω_1, the main frequency of the cycle. Soon

after that a chaotic structure nucleates in the core of the soliton and subsequently spreads over the entire axis. Fig. 5 shows a typical evolution of the soliton in the spatiotemporal chaotic domain.

We conclude the discussion of the observations by mentioning a few curious phenomena the explanation of which will be given elsewhere. First, it is worthwhile to notice an unusual, "shark jaw" shape of the boundary between the regions of the zero attractor and spatio-temporal chaos. Second, we have simulated the evolution of the unstable *homogeneous* solution of eq. (3) at some points of the zero attractor domain between the lines 2 and 4. Surprisingly, the result of this evolution was an equidistant sequence of stationary solitons. Finally for small γ and several h, the soliton was seen to start travelling over a background radiation. This was observed e.g. for $\gamma = 0.01, h = 0.087$.

It is natural to expect that our results will remain valid for small-amplitude breathers of the parametrically driven, damped Landau-Lifshitz and sine-Gordon equations [11, 3]. In particular, we know that the sine-Gordon equation

$$u_{\tau\tau} + \lambda u_\tau - u_{zz} + (1 - f\cos 2\omega\tau)\sin u = 0 \qquad (5)$$

with the driving frequency ω such that $1 - \omega^2 \equiv \epsilon^2 \ll 1$, reduces [3] to eq. (3) with $x = \epsilon z$, $t = \epsilon^2\tau/2$, $h = f/(2\epsilon^2)$, $\gamma = \lambda/\epsilon^2$, and $u(\tau, z) = -4\epsilon\mathrm{Re}\left[i\phi(t,x)e^{-i\omega\tau}\right]$. Note that the length of the sine-Gordon interval of integration, L_{SG}, and the NLS interval L_{NLS} are related as $L_{SG} = (1/\epsilon)L_{NLS}$. Consequently, our NLS results with $L_{NLS} = 50$ correspond to the integration of the sine-Gordon equation (5) with e. g. $\omega = 0.98$ on the interval $L_{SG} \approx 250$.

At this point, it is interesting to make contact with two closely related systems, namely the *directly* driven sine-Gordon and NLS equations. Different groups reported observations of different scenarios of transition to chaos in these systems [15, 16, 17, 18, 19]. In the case of the driven sine-Gordon in the NLS limit, for instance, Taki *et al* [18] observed the period-doubling route while Bishop *et al* [16] reported the quasiperiodic transition. The difference in the observed scenarios has been generally attributed to the fact that the values of the driver's strength and

dissipation coefficient examined in [16] and [18], differ by order of magnitude. Consequently, the question of the interface between the two scenarios did not arise. However transforming the sine-Gordon to the NLS as it was done above, one can easily verify that in terms of the NLS control parameters the period-doubling and quasiperiodic transitions occur in a close proximity. (Namely, the line of the period doublings observed in [18] corresponds to $\gamma \approx 0.12$ whereas the quasiperiodic transition of [16] pertains to $\gamma \approx 0.16$.) Therefore the finding of the mutual arrangement and interface between the regions of the two types of transition on the attractor chart of the above equations, becomes an important problem. Figure 1 gives a complete solution to a similar problem in the case of the *parametrically* driven NLS. Given the fact that the two equations have the same mechanism of the soliton instability [20, 3], it would be interesting to check whether the period-doubling and quasiperiodic routes meet at a "tricritical" point in the directly driven NLS as well. This work is in progress.

To summarise, we numerically studied nonlinear oscillations and chaotisation of the parametrically driven NLS soliton in the domain where the stationary soliton is unstable. Using this unstable soliton as an initial condition, we found a variety of spatially localised and extended attractors, obtained their quantitative characteristics, and compiled the attractor chart on the (h, γ) plane.

Acknowledgments.

We are grateful to B.Herbst, A.Weideman, C.Bondila, E.Brüning, A.Harin, I.V. Puzynin, A.M.Kosevich and J.Ronda for their generous assistance in the course of this work. One of the authors (M.Bondila) wishes to especially thank Ben and Hendrina Herbst for their hospitality in Bloemfontein and Rudy Bock at CERN. M.Bogdan acknowledges support from the Visiting Lecturer's Fund of UCT and Laboratory for Computing Techniques of JINR. This research was supported by FRD of South Africa, an International Soros Foundation grant (No.U2I000), two grants from SCST of Ukraine (2.3/640 and 2.2/142), and a research grant from the University Research Council of UCT.

Figure Captions

Fig. 1

The attractor chart of eq. (3) on the (h, γ)-plane. Below the line $h < \gamma$ there are no localised solutions, and the only attractor is $\phi \equiv 0$. Above the line $h = (1+\gamma^2)^{1/2}$ the zero solution is unstable with respect to the excitation of continuous spectrum waves. In the area between these two lines, we used empty circles to denote period-1 solutions and shadowed boxes for periods-2, 4, and 8. Small white blobs indicate period-6, period-7 and period-10 solitons observed at $(\gamma = 0.262, h = 0.46)$, $(\gamma = 0.235, h = 0.355)$ and $(\gamma = 0.18, h = 0.251)$, respectively. Finally, shadowed diamonds stand for type-I and type-II strange attractors observed at $(\gamma = 0.18, h = 0.253)$ and $(\gamma = 0.26, 0.4530 < h < 0.4539)$, respectively, as well as for complex cycles. The region of stable stationary solitons is left blank; empty triangles mark the area where the only attractor is $\phi \equiv 0$, and the domain of spatio-temporal chaos is marked by black triangles. Note an unexpectedly complex, "shark jaw" shape of the interface between the regions of spatio-temporal chaos and zero attractor.

Fig. 2

An enlarged portion of Fig. 1 displaying the period-doubling route to chaos. Notation is as in Fig. 1 with the exception that shadowed boxes, triangles, and circles stand for periods-2, 4, and 8, respectively. The black blob at $\gamma = 0.262, h = 0.46$ marks a period-6 solution.

Fig. 3

Power spectral densities. a-d: periods-1, 2, 4, 8. e: 2-band strange attractor.

Fig. 4

a,b: type-I (two-band) strange attractor, $\gamma = 0.26, h = 0.453974$. c,d: type-II strange attractor, $\gamma = 0.18, h = 0.253$. e: the crisis of the strange attractor, $\gamma = 0.26, h = 0.453975$.

Fig. 5

Spatio-temporal chaos seeded by the soliton.

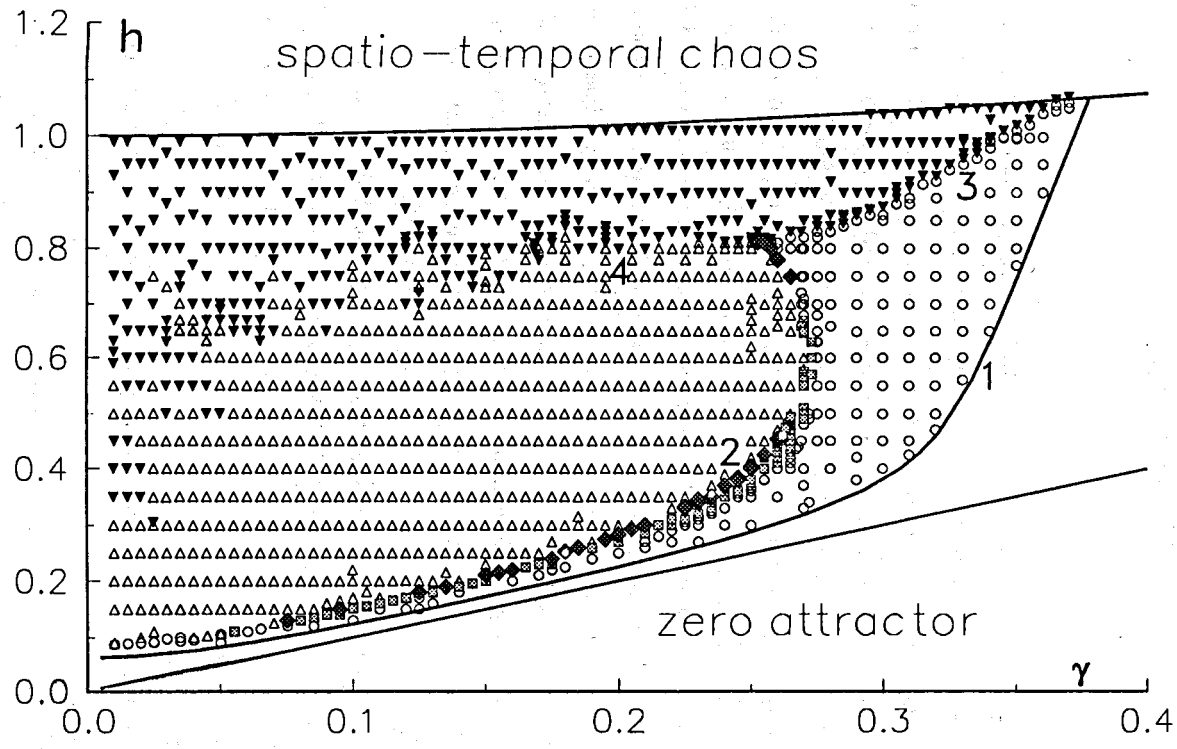
h
spatio–temporal chaos
zero attractor
1
2
3
4
γ
1.2
1.0
0.8
0.6
0.4
0.2
0.0
0.0
0.1
0.2
0.3
0.4

Fig. 1

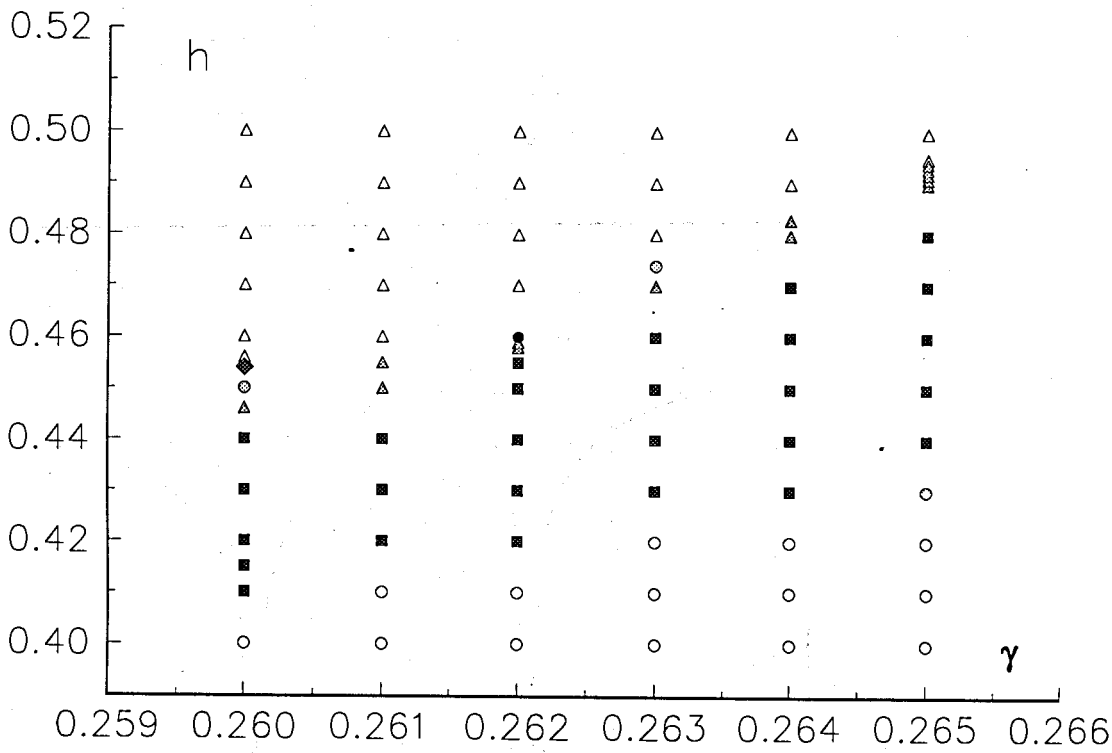
h
γ
0.52
0.50
0.48
0.46
0.44
0.42
0.40
0.259
0.260
0.261
0.262
0.263
0.264
0.265
0.266

Fig. 2

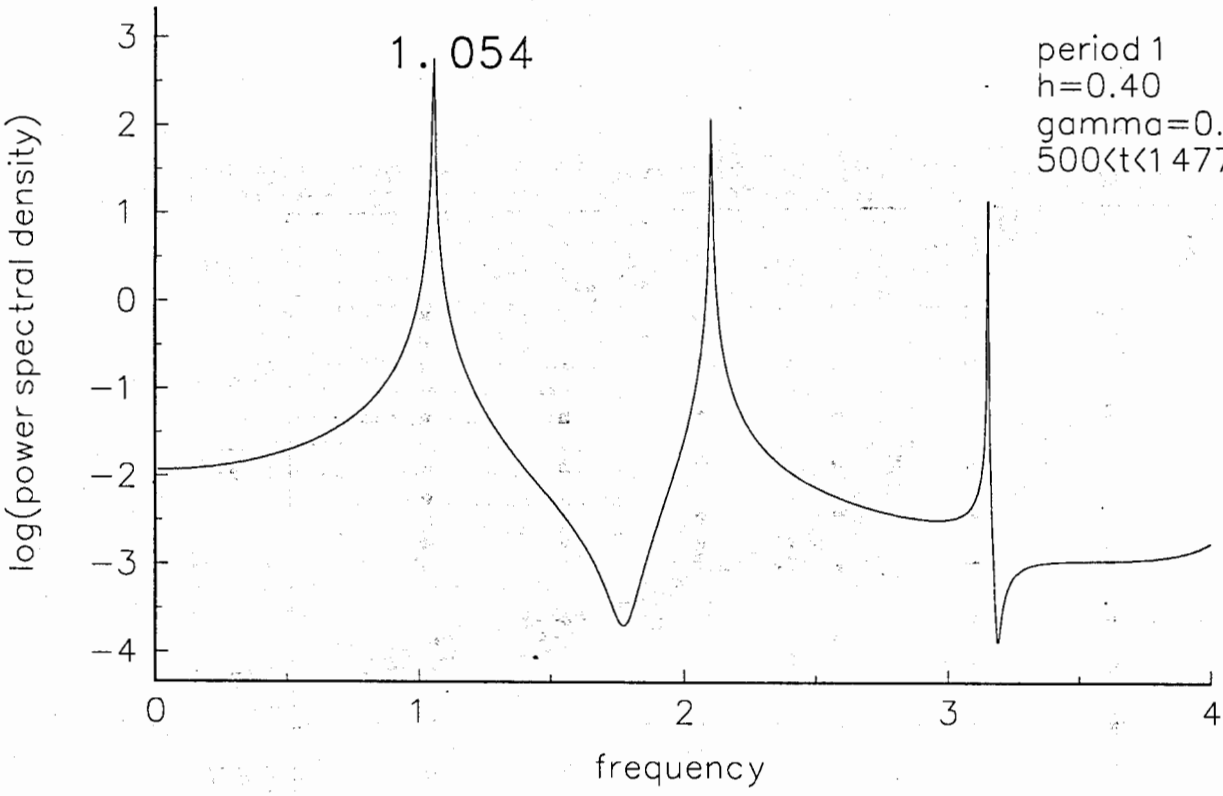
1.054
period 1
h=0.40
gamma=0.26
500<t<1477
log(power spectral density)
frequency
3
2
1
0
−1
−2
−3
−4
0
1
2
3
4

Fig.3a

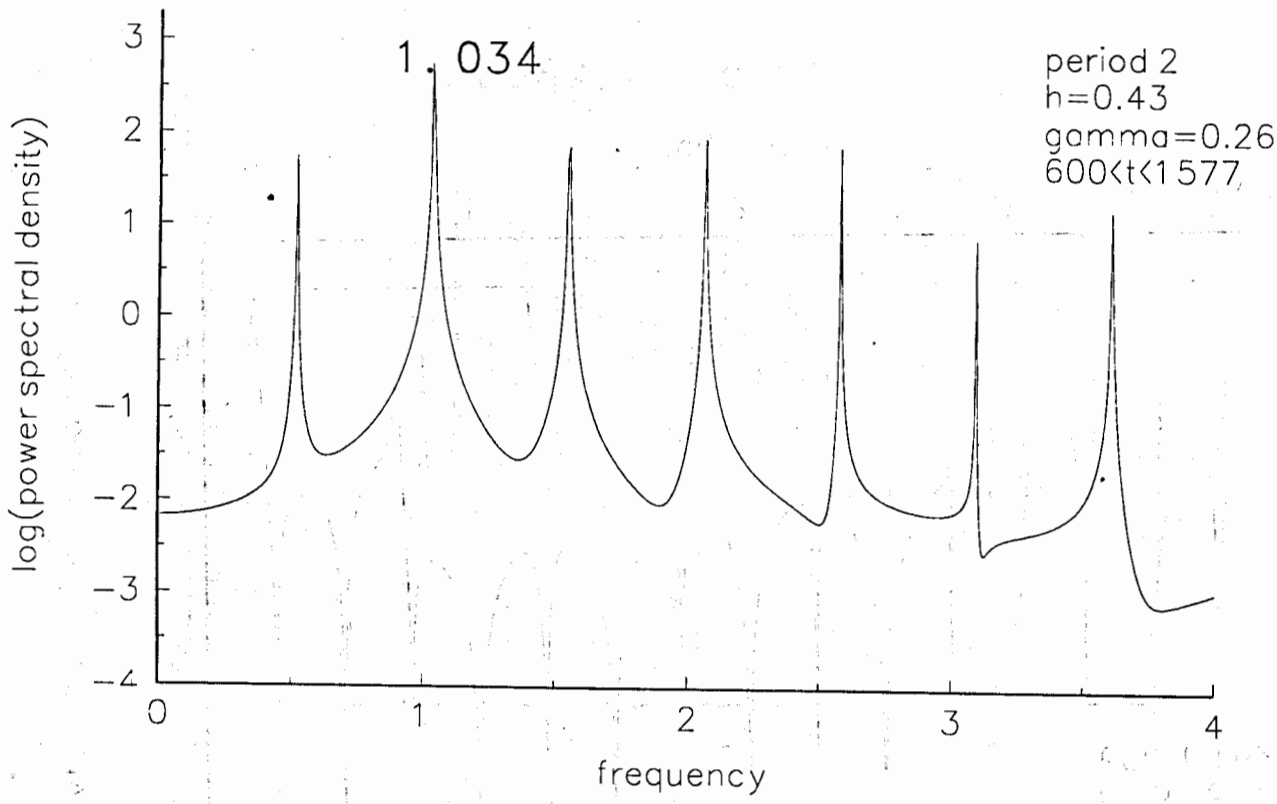
1.034
period 2
h=0.43
gamma=0.26
600<t<1577
log(power spectral density)
frequency
3
2
1
0
−1
−2
−3
−4
0
1
2
3
4

Fig.3b

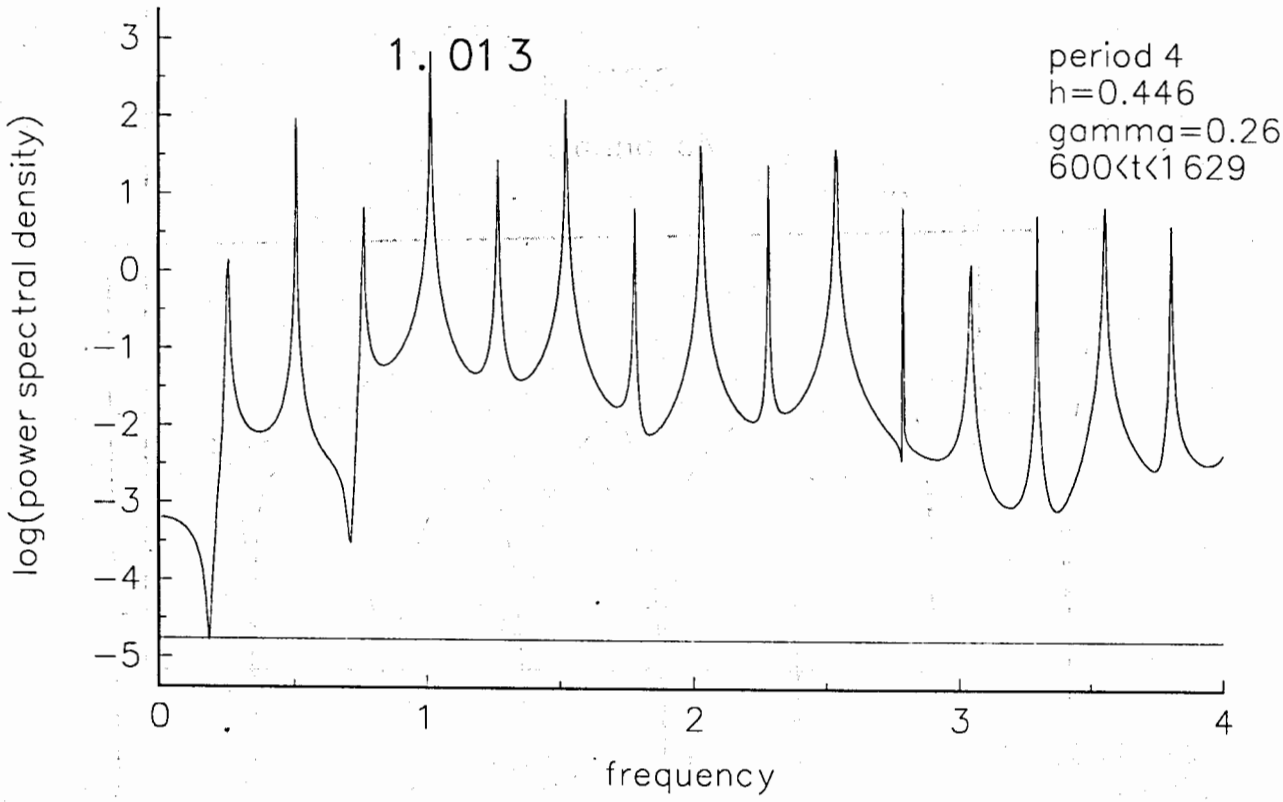
1.013
period 4
h=0.446
gamma=0.26
600<t<1629
log(power spectral density)
frequency
3
2
1
0
−1
−2
−3
−4
−5
0
1
2
3
4

Fig.3c

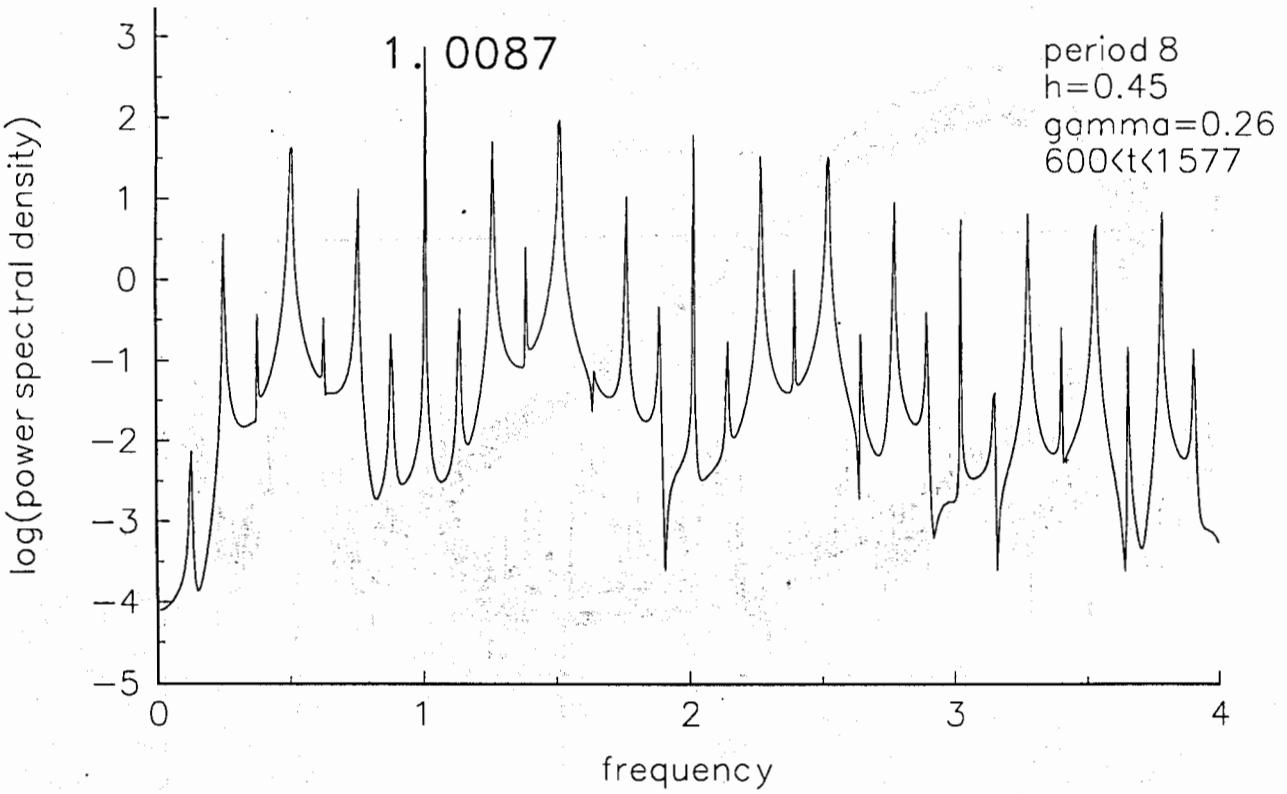
1.0087
period 8
h=0.45
gamma=0.26
600<t<1577
log(power spectral density)
frequency
3
2
1
0
−1
−2
−3
−4
−5
0
1
2
3
4

Fig.3d

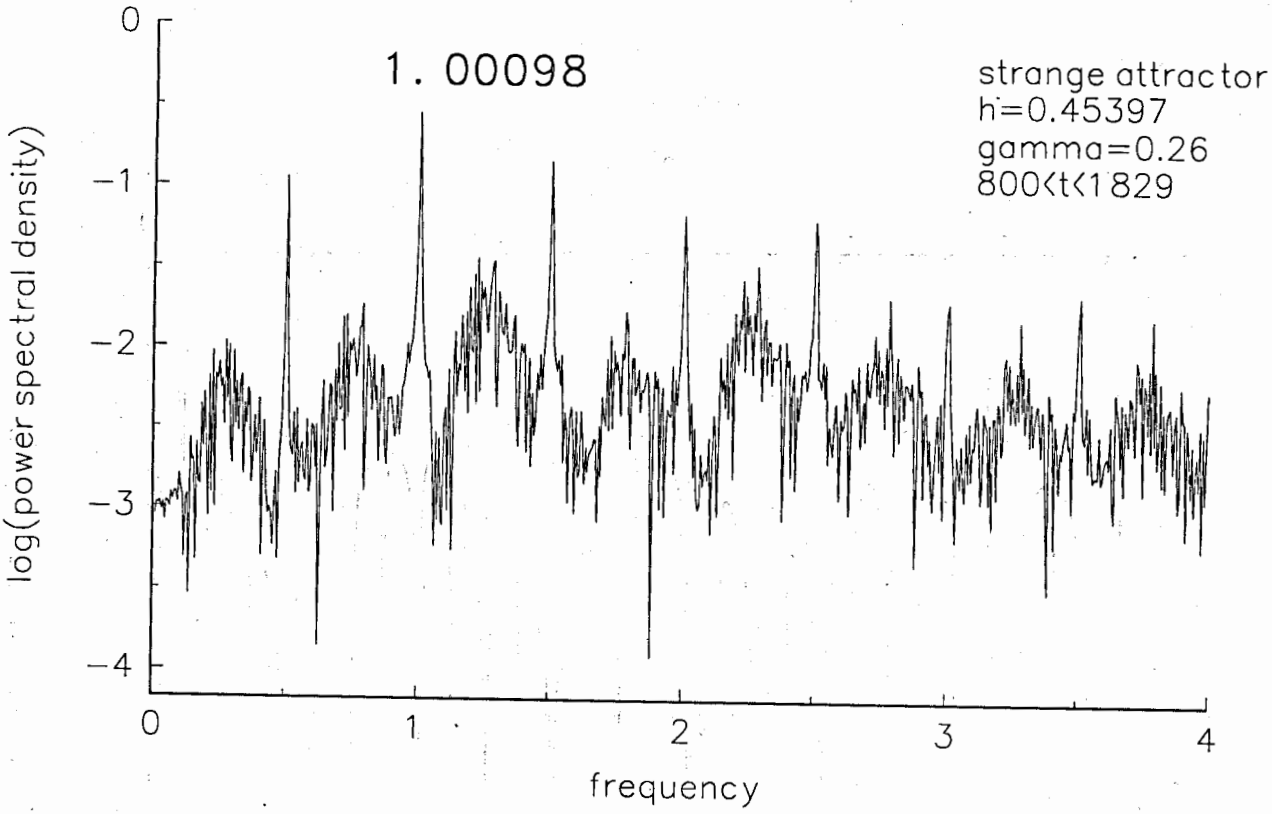
1. 00098
strange attractor
h=0.45397
gamma=0.26
800<t<1829
log(power spectral density)
0
−1
−2
−3
−4
0
1
2
3
4
frequency

Fig.3e

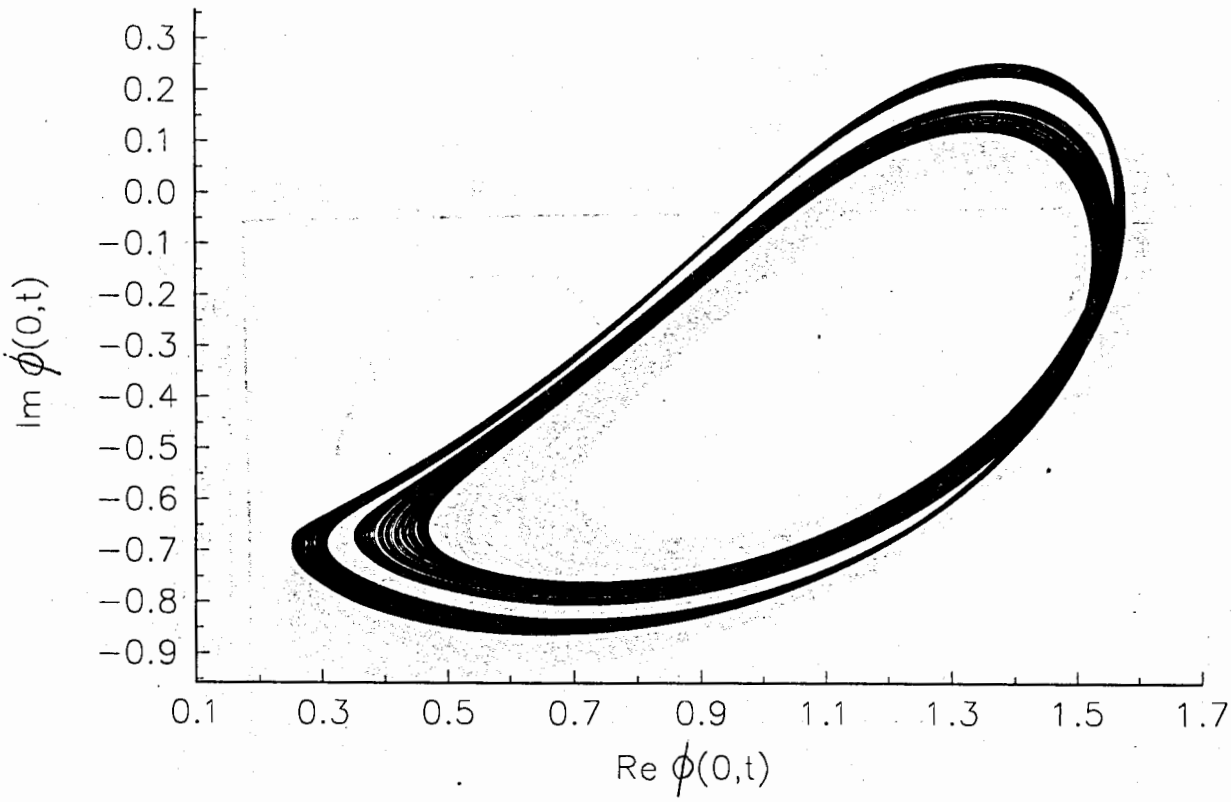
Im φ(0,t)
0.3
0.2
0.1
0.0
−0.1
−0.2
−0.3
−0.4
−0.5
−0.6
−0.7
−0.8
−0.9
0.1
0.3
0.5
0.7
0.9
1.1
1.3
1.5
1.7
Re φ(0,t)

Fig.4a

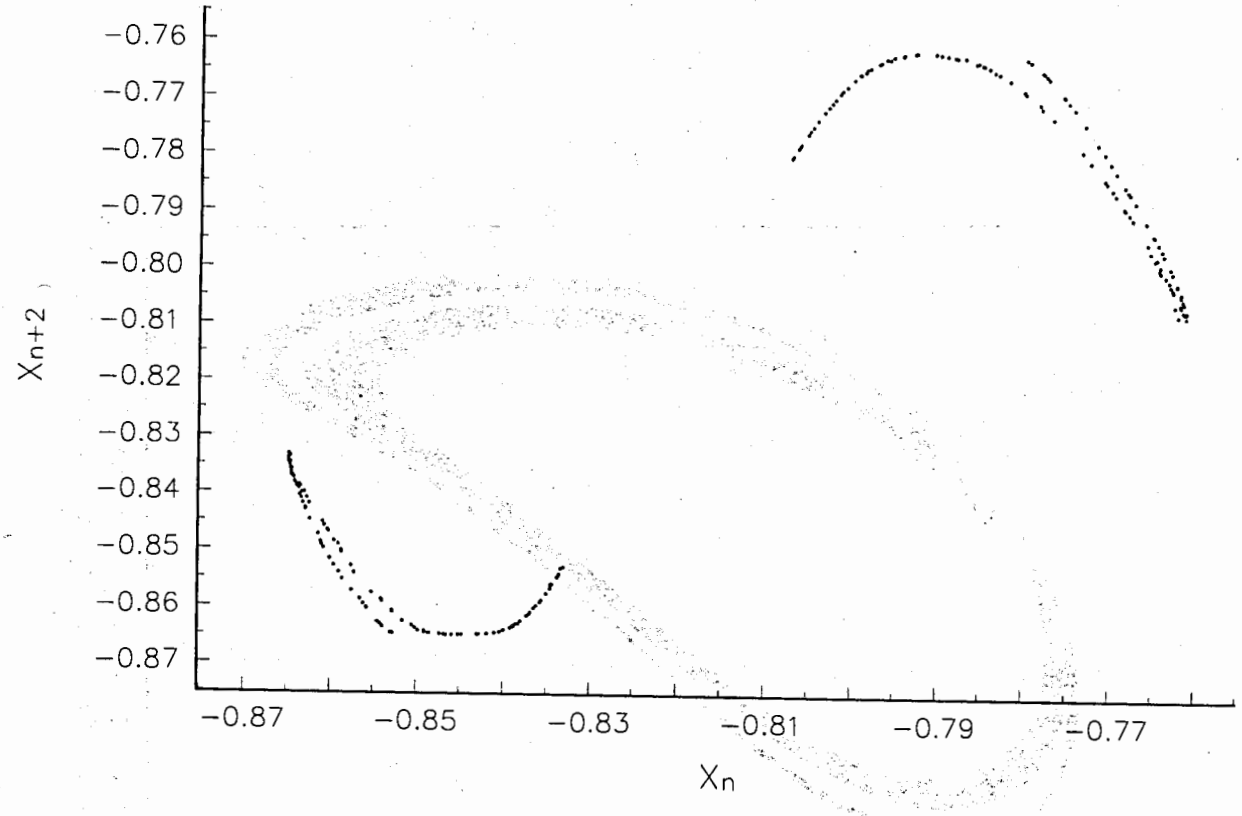
−0.76
−0.77
−0.78
−0.79
−0.80
−0.81
−0.82
−0.83
−0.84
−0.85
−0.86
−0.87
Xn+2
−0.87
−0.85
−0.83
−0.81
−0.79
−0.77
Xn

Fig.4b

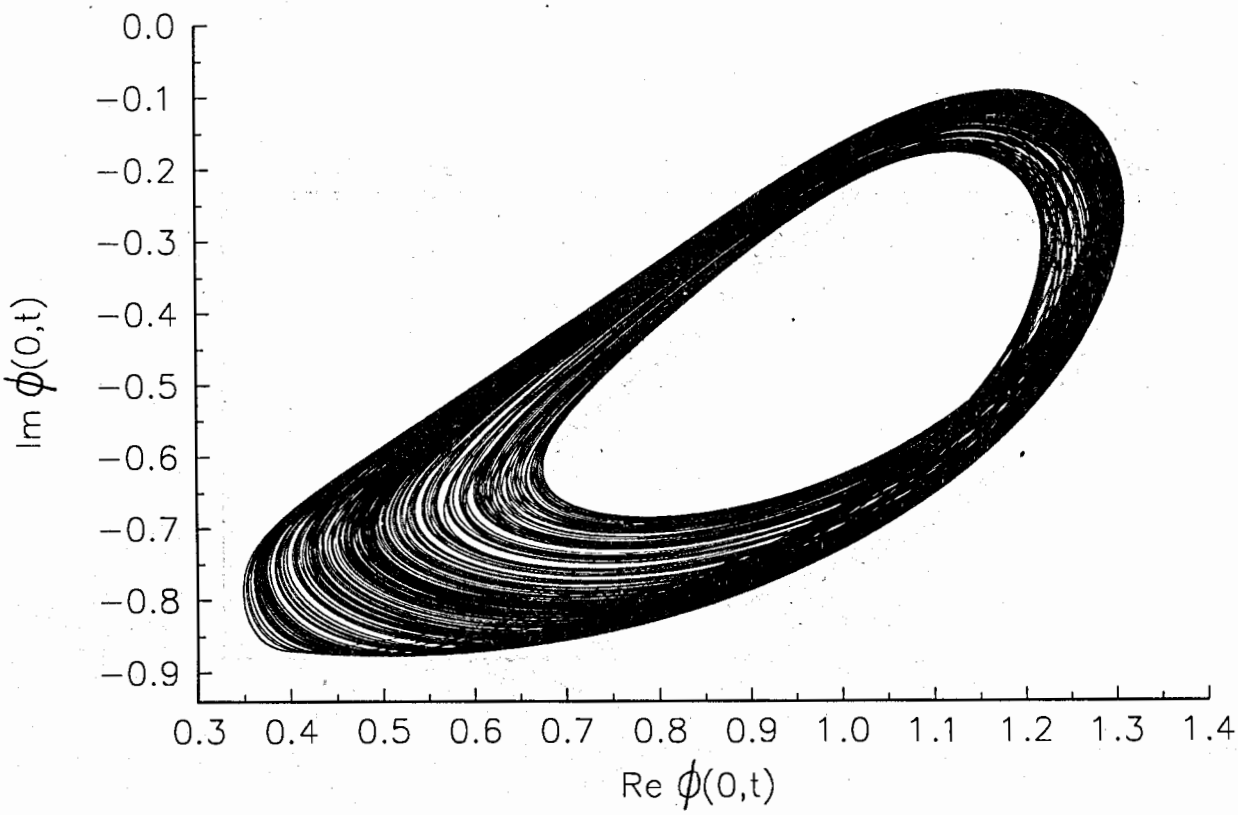
0.0
−0.1
−0.2
−0.3
−0.4
−0.5
−0.6
−0.7
−0.8
−0.9
Im φ(0,t)
0.3
0.4
0.5
0.6
0.7
0.8
0.9
1.0
1.1
1.2
1.3
1.4
Re φ(0,t)

Fig.4c

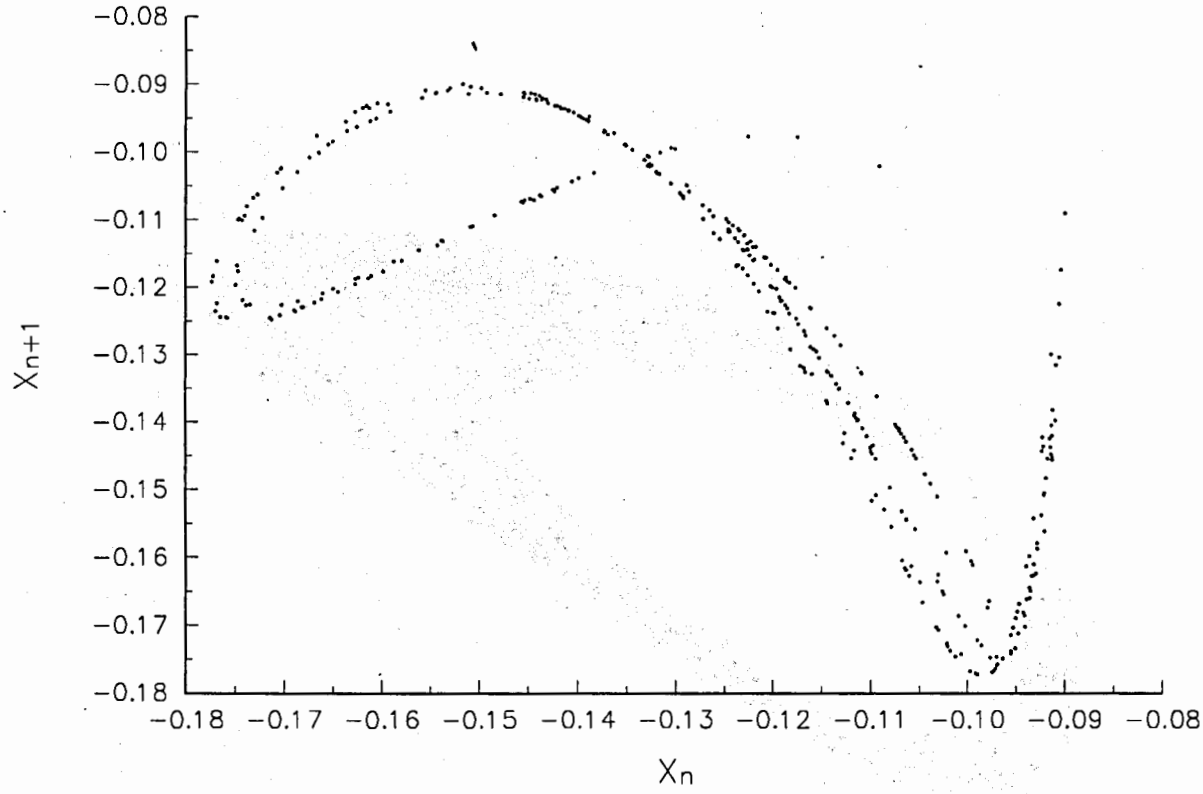
−0.08
−0.09
−0.10
−0.11
−0.12
−0.13
−0.14
−0.15
−0.16
−0.17
−0.18
Xn+1
−0.18 −0.17 −0.16 −0.15 −0.14 −0.13 −0.12 −0.11 −0.10 −0.09 −0.08
Xn

Fig. 4d

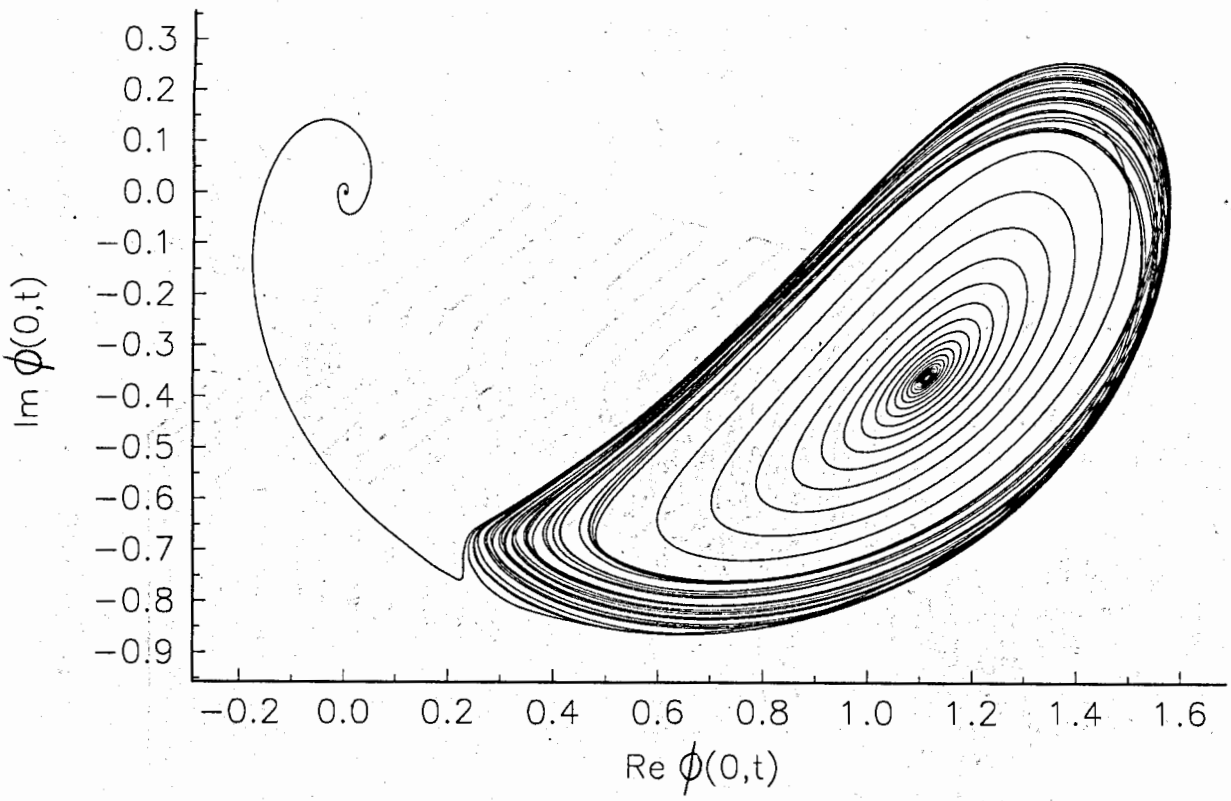
0.3
0.2
0.1
0.0
−0.1
−0.2
−0.3
−0.4
−0.5
−0.6
−0.7
−0.8
−0.9
Im φ(0,t)
−0.2 0.0 0.2 0.4 0.6 0.8 1.0 1.2 1.4 1.6
Re φ(0,t)

Fig.4e

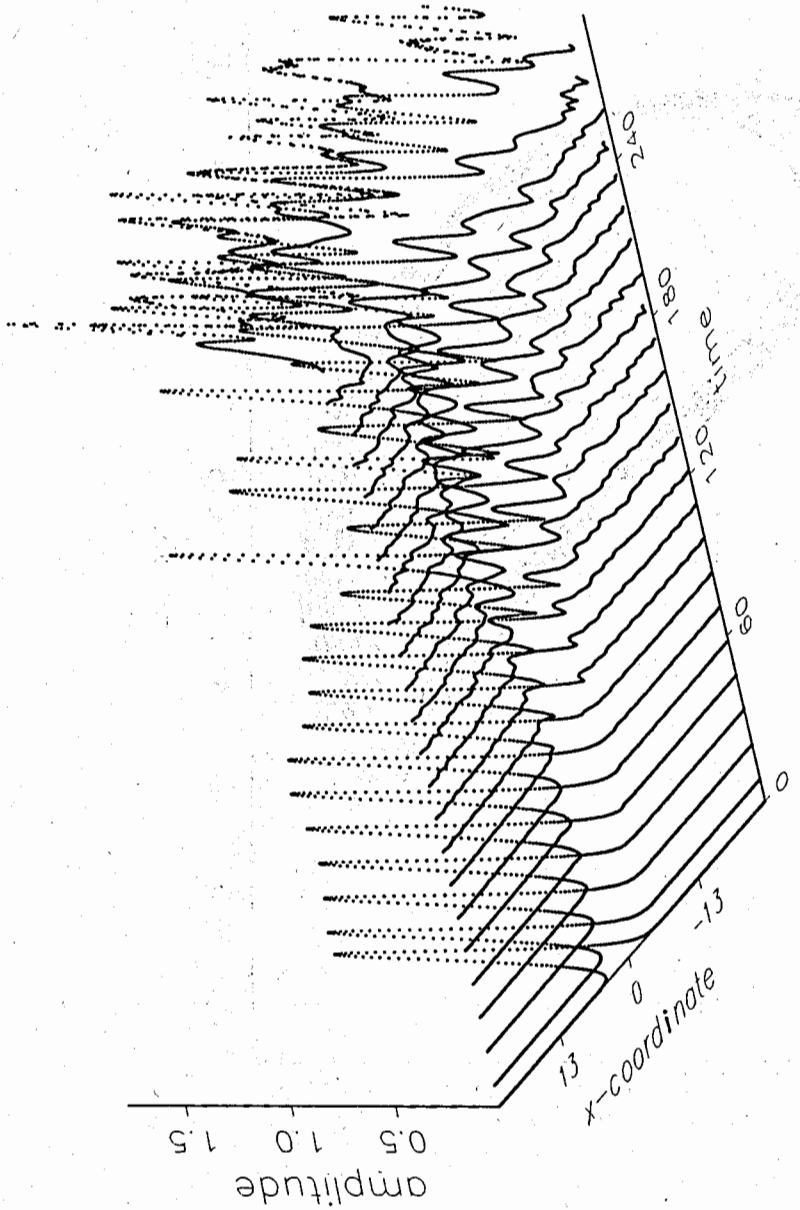

Fig.5

References

[1] V.E. Zakharov, V.S. L'vov and S.S. Starobinets, Sov. Phys. Uspekhi **17**, 896 (1975); V.S. L'vov *et. al.*, Fizika Tverdogo Tela **15**, 793 (1973)

[2] J.W. Miles, J. Fluid. Mech. **148**, 451 (1984)

[3] I.V.Barashenkov, M.M.Bogdan, V.I.Korobov, Europhys. Lett. **15**, 113 (1991)

[4] J. Wu, R. Keolian, and I. Rudnick, Phys. Rev. Lett. **52**, 1421 (1984)

[5] H. Yamazaki and M. Mino, Progr. Theor. Phys. Suppl. **98**, 400 (1989)

[6] V. E. Zakharov, S. L. Musher and A. M. Rubenchik, Phys. Rep. **129**, 285 (1985)

[7] N. Yajima and M. Tanaka, Prog. Theor. Phys. Suppl. **94**, 138 (1988)

[8] C. Vanneste et.al., J. Low Temp. Phys. **45**, 517 (1981); see also G. Cicogna and L. Fronzoni, Phys. Rev. **A42**, 1901 (1990)

[9] G. Wysin and A. R. Bishop, J. Magn. & Magn. Mater. **54-57**, 1132 (1986)

[10] M. V. Goldman, Rev. Mod. Phys. **56**, 709 (1984); E.A. Kuznetsov, A.M. Rubenchik, and V.E. Zakharov, Phys. Rep. **142**, 103 (1986)

[11] M.M. Bogdan, A.M. Kosevich and I.V. Manzhos, Sov. J. Low Temp. Phys. **11**, 547 (1985)

[12] For $\gamma < h < (1+\gamma^2)^{1/2}$, there is another soliton solution given by almost the same formulas (4). The only difference is that this time, the phase is $\theta = \pi/2 - \arcsin\gamma/h$. We disregard this solution here as it is unstable for all h and γ [3].

[13] It is interesting to note that the same mechanism of the soliton instability occurs in the *directly* driven NLS [20].

[14] J. A. C. Weideman and B. M. Herbst, SIAM J. Numer. Anal. **23**, 485 (1986).

[15] K. Nozaki and N. Bekki, Physica **D21**, 381 (1986)

[16] A. R. Bishop, M. G. Forest, D. W. Mclaughlin, E. A. Overman II, Physica **23D**, 293 (1986)

[17] K. H. Spatschek, H. Pietsch, E. W. Laedke and Th. Eickermann. In: *Singular Behaviour and Nonlinear Dynamics.* T. Bountis and St. Pnevmatikos, Eds. World Sci. (1989)

[18] M. Taki, K. H. Spatschek, J. C. Fernandez, R. Grauer and G. Reinisch, Physica **D40**, 65 (1989)

[19] G.Terrones, D.W.McLaughlin, and A.J.Pearlstein. Preprint of the University of Arizona, Tucson (1989)

[20] I.V. Barashenkov, M.M. Bogdan, T. Zhanlav. In: *Nonlinear World: IV International Workshop on Nonlinear and Turbulent Processes in Physics. Kiev, 9-22 October 1989.* V.G.Bar'yakhtar *et.al.*, eds. World Sci. (1990), p.3

Received by Publishing Department
on January 30, 1995.

Бондила М., Барашенков И.В., Богдан М.М. E5-95-30

Топография аттракторов нелинейного уравнения Шредингера с параметрической накачкой

Нелинейное уравнение Шредингера с параметрической накачкой и диссипацией численно исследовано в окрестности его точного солитонного решения. Получена карта аттракторов в области неустойчивости солитона на плоскости управляющих параметров. Обнаружены подобласти, в которых переход к хаосу происходит через удвоение периода и через квазипериодичность, и продемонстрировано существование критической точки, где два сценария смыкаются.

Работа выполнена в Лаборатории вычислительной техники и автоматизации ОИЯИ.

Препринт Объединенного института ядерных исследований. Дубна, 1995

Bondila M., Barashenkov I.V., Bogdan M.M. E5-95-30

Topography of Attractors of the Parametrically Driven Nonlinear Schrödinger Equation

The parametrically driven, damped NLS equation is numerically simulated in the neighborhood of its exact soliton solution. We obtain the attractor chart on the control parameter plane in the domain of the soliton instability. Regions of the period-doubling and quasiperiodic transitions to chaos are found, and the existence of a critical point where the two scenarios meet, is demonstrated.

The investigation has been performed at the Laboratory of Computing Techniques and Automation, JINR.

Preprint of the Joint Institute for Nuclear Research. Dubna, 1995